



RESEARCH ARTICLE | SEPTEMBER 23 2024

## Anti-diffusion method for coupled level set and volume of fluid, volume of fluid, and tangent of hyperbola for interface capturing methods

Kensuke Yokoi  



*Physics of Fluids* 36, 092121 (2024)

<https://doi.org/10.1063/5.0223722>



### Articles You May Be Interested In

A coupled level-set and tangent of hyperbola interface capturing (THINC) scheme with a single-step time integration for incompressible flows

*Physics of Fluids* (November 2023)

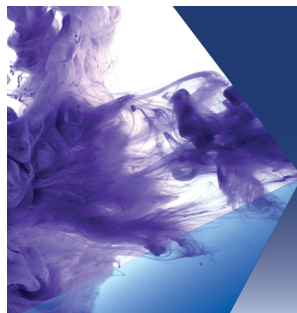
A coupling algorithm of the coupled level set and volume of fluid/immersed boundary method and adaptive mesh refine method for simulating multiphase flows

*Physics of Fluids* (September 2024)

Numerical simulations for incompressible turbulence cavitation flows with tangent of hyperbola interface capturing (THINC) scheme

*Physics of Fluids* (February 2022)

01 October 2024 13:03:21



## Physics of Fluids

Special Topic:

Recent Advances in Fluid Dynamics and its Applications

Guest Editors: B.Reddappa, B. Rushi Kumar, Sreedhara Rao Gunakala, Bijula Prabhakar Reddy

[Submit Today!](#)

# Anti-diffusion method for coupled level set and volume of fluid, volume of fluid, and tangent of hyperbola for interface capturing methods

Cite as: Phys. Fluids **36**, 092121 (2024); doi: 10.1063/5.0223722

Submitted: 17 June 2024 · Accepted: 29 August 2024 ·

Published Online: 23 September 2024



View Online



Export Citation



CrossMark

Kensuke Yokoi<sup>a)</sup> 

## AFFILIATIONS

School of Engineering, Cardiff University, The Parade, Cardiff CF24 3AA, United Kingdom

<sup>a)</sup> Author to whom correspondence should be addressed: [Yokoik@cardiff.ac.uk](mailto:Yokoik@cardiff.ac.uk)

## ABSTRACT

In this paper, we propose an anti-diffusion method to effectively prevent flotsams (non-physical tiny droplets and bubbles) and/or diffusion of the VOF (volume of fluid) function that occur in CLSVOF (coupled level set and volume of fluid), VOF (volume of fluid), and THINC (tangent of hyperbola for interface capturing) methods. In the proposed method, VOF functions that are not 1 or 0 and exist at a certain distance from the interface are identified as flotsams and/or diffusion ( $C_{ad}$ ), and these VOF functions ( $C_{ad}$ ) are moved to the transition region around the interface, where the VOF value is between 0 and 1, using a conservative advection method to prevent flotsams and/or diffusion. Additionally, the proposed method allows for some control over the position to which  $C_{ad}$  is moved within the transition region. As a result of applying the proposed anti-diffusion method to various benchmark tests and droplet problems, it was found that the proposed method effectively suppresses flotsams and/or diffusion while ensuring conservation. In some cases, the anti-diffusion method even improves interface capture accuracy. Furthermore, investigating the impact of the position to which  $C_{ad}$  is moved revealed that when handling  $C_{ad}$  occurring on the gas side (liquid side), moving  $C_{ad}$  as far as possible from the gas side (liquid side) increases the effectiveness of flotsams suppression.

© 2024 Author(s). All article content, except where otherwise noted, is licensed under a Creative Commons Attribution (CC BY) license (<https://creativecommons.org/licenses/by/4.0/>). <https://doi.org/10.1063/5.0223722>

## I. INTRODUCTION

The volume of fluid (VOF) method<sup>6,12,16,22,24</sup> is a numerical simulation technique used to capture interfaces in two-phase fluid flows. It represents the interface by using the volume fraction of fluid in each grid cell. This method effectively preserves the interface shape and ensures mass conservation. The VOF method has been used for multiphase flow simulations in a wide range of science and engineering fields, including physics, applied mathematics, mechanical engineering, civil engineering, chemical engineering, and others. In the VOF method, a stepped Heaviside function of 0 or 1 is used as the interface capturing function. Recently, the THINC (tangent of hyperbola for interface capturing) method,<sup>7,30,34,36</sup> which uses a smoothed Heaviside function instead of the stepped Heaviside function, has also become widely used. Like the VOF method, the THINC method can precisely maintain the interface shape while ensuring mass conservation. The CLSVOF (coupled level set and volume of fluid) method<sup>25,29,33,35</sup> combines the level set method<sup>21,26</sup> with the VOF (or THINC) method. The CLSVOF method retains the conservation properties and high interface capturing accuracy of the VOF method, while also incorporating

the advantages of the level set method, such as curvature calculations and surface tension calculations. As a result, the CLSVOF method is widely used by many researchers alongside the VOF method. In this paper, the CLSVOF method is adopted for interface capturing. For the advection calculation of the VOF function in the CLSVOF method, both the THINC/WLIC (weighted line interface calculation) and VOF/WLIC methods<sup>36</sup> are employed.

However, the VOF method, the THINC method, and the CLSVOF method have the issue of generating artificial small droplets and/or bubbles, which will henceforth be referred to as flotsams<sup>23,27</sup> [e.g., see Figs. 9(a) and 16(a)]. This issue of flotsams becomes particularly pronounced in multiphase flow problems involving large deformations of the interface. Additionally, some numerical diffusion may occur around the interface depending on the situation. To address these issues, a method called truncation<sup>25</sup> has been proposed for the CLSVOF method. This method forces the flotsams and numerical diffusion that appear at a certain distance from the interface (e.g., one mesh spacing) to be set to 0 or 1, which raises the problem of not guaranteeing the conservation of the VOF function (however, the amount

of generated flotsams and/or diffusion is generally not very large (depending on the situation), so the conservation error is very limited). Therefore, this paper proposes a method to handle flotsams and numerical diffusion while fully satisfying the conservation law. The VOF, THINC, and CLSVOF methods are widely used by numerous researchers across various fields of study. We are confident that the proposed method will contribute to the improvement of numerical simulations of multiphase flows using VOF, THINC, and CLSVOF methods.

To the best of my knowledge, there is no existing anti-diffusion method for VOF and THINC methods. Here, VOF and THINC methods refer to the geometric VOF and THINC methods that perform geometric interface reconstruction and do not include methods that combine general advection solvers with anti-diffusion (while methods using general advection equation solver are superior in terms of versatility, when purely comparing the performance of interface capturing, geometric VOF and THINC methods have advantages). This is likely due to the fact that numerical diffusion in geometric VOF and THINC methods is significantly smaller than that in general advection equation solvers (however, the diffusion is not entirely absent, and the issue of flotsams, which does not occur in methods solving general advection equations, do arise), and in the case of VOF method, the interface thickness is one mesh (mathematically zero), which is extremely thin.

This paper proposes an anti-diffusion technique that suppresses flotsams and/or numerical diffusion in the CLSVOF method while satisfying conservation. In the proposed method, similar to truncation in the CLSVOF method, deviations of the VOF function from 0 or 1 that occur at a distance greater than a certain threshold from the interface (e.g., 1–1.5 mesh spacing) are defined as flotsams and/or diffusion ( $C_{ad}$ ).  $C_{ad}$  is then moved into the transition region (where the VOF function is between 0 and 1) near the interface using the normal vector to the interface calculated by the level set function. This approach prevents flotsams and/or diffusion while ensuring conservation. Moreover, the proposed method allows flotsams and/or diffusion to be moved to any location within the transition region of the interface (specifically, the distance from the interface to the location where they are moved can be specified). This enables the investigation of the effects of different locations for moving  $C_{ad}$ . A similar method may be the phase field model,<sup>3,10,18</sup> but unlike the VOF method, the phase field model does not reconstruct the interface. While the phase field model includes an anti-diffusion effect, the application of anti-diffusion in the phase field model is significantly different from that in the proposed method. The STAA (surface tracking by artificial anti-diffusion) method<sup>31</sup> is also similar to the proposed method, but it was proposed for use with conventional advection solvers such as CIP–CSL scheme<sup>13,14,20,32</sup> for interface capturing and has not been applied to the VOF method. The STAA method is briefly explained only as a part of the paper focused on applications of free surface flows, and its details are unclear.

In this paper, we propose an anti-diffusion technique for the CLSVOF method (also the VOF method and the THINC method). The details of the anti-diffusion method are given in Sec. II. In Sec. III, numerical results of advection tests (Zalesak problem and single vortex flow test) and free surface flow tests (coalescence and separation of liquid droplets of  $We = 23$  and  $24$ ) are given. The summary is given in Sec. IV.

## II. NUMERICAL METHOD

### A. Interface capturing

For interface capturing, the CLSVOF method<sup>25,35</sup> is used. In combination with the CLSVOF method, the THINC/WLIC method<sup>36</sup> and the VOF/WLIC method<sup>36</sup> are used as a VOF method. First, the volume fraction  $C_{i,j}$ ,

$$C_{i,j} = \frac{1}{\Delta x \Delta y} \int_{\Omega_{i,j}} \chi(x, y) d\Omega, \quad (1)$$

is updated using the THINC/WLIC scheme or the VOF/WLIC method by solving the following advection equation:

$$\frac{\partial \chi}{\partial t} + \nabla \cdot (\mathbf{u}\chi) - \chi \nabla \cdot \mathbf{u} = 0, \quad (2)$$

where  $\chi$  is the characteristic function, and the cell average of  $\chi$  is the volume fraction  $C_{i,j}$ .  $\mathbf{u}$  is the velocity. In the THINC method, we can set the thickness of the interface; therefore, in this paper, the thickness of the interface is set to  $3\Delta$  (here,  $\Delta = \Delta x = \Delta y$ ). In the VOF method, the stepped Heaviside function (zero thickness) is used. Then, the level set function  $\psi_{i,j}$  is created based on interface which is indicated by  $C_{i,j}$  ( $C_{i,j} = 0.5$ ).<sup>25,35</sup> The level set function satisfies

$$|\nabla \psi| = 1 \text{ for whole region}, \quad (3)$$

and

$$\psi = \begin{cases} > 0 & \text{for the liquid} \\ = 0 & \text{at the interface} \\ < 0 & \text{for the gas.} \end{cases} \quad (4)$$

The unit normal vector to the liquid interface can be calculated using the level set function as follows:

$$\mathbf{n}_{ls} = \frac{\nabla \psi}{|\nabla \psi|}. \quad (5)$$

The density (color) function  $\phi_d$  which is used to define the physical properties for different materials, such as density and viscosity, can be created by using a smoothed Heaviside function

$$\phi_d = H_\alpha(\psi) \quad (6)$$

with

$$H_\alpha(\psi) = \begin{cases} 0 & \text{if } \psi < -\alpha \\ \frac{1}{2} \left[ 1 + \frac{\psi}{\alpha} + \frac{1}{\pi} \sin\left(\frac{\pi\psi}{\alpha}\right) \right] & \text{if } |\psi| \leq \alpha \\ 1 & \text{if } \psi > \alpha, \end{cases} \quad (7)$$

where  $2\alpha$  represents the thickness of the transition region between the liquid phase and the gas phase. In this paper,  $\alpha = 1.5\Delta x$  was used. The density function is set as  $\phi_d = 1$  for the liquid and  $\phi_d = 0$  for the gas. The density  $\rho$  and the viscosity  $\mu$  are calculated as follows:

$$\rho = \rho_{liquid}\phi_d + \rho_{air}(1 - \phi_d), \quad (8)$$

$$\mu = \mu_{liquid}\phi_d + \mu_{air}(1 - \phi_d), \quad (9)$$

where  $\rho_{liquid}$  and  $\rho_{air}$  are the densities of liquid and air, and  $\mu_{liquid}$  and  $\mu_{air}$  are the viscosities of liquid and air, respectively. In this paper, the

density and viscosity coefficient were calculated using Eqs. (8) and (9), but these can also be calculated directly using  $C$  instead of  $\phi_d$  in Eqs. (8) and (9). In this paper, the VOF function, the level set function, the density function, the density, and the viscosity are defined only at cell centers. When some other variables which are not defined at cell centers like  $\rho_{i+1/2,j}$  are required, we calculate these using simple averaging procedures like  $\rho_{i+1/2,j} = \frac{\rho_{ij} + \rho_{i+1,j}}{2}$ .

**B. Anti-diffusion algorithm for the CLSVOF method (CLSVOF-AD method)**

In this section, we explain the detail of the anti-diffusion algorithm. First, we assume the followings:

- The VOF method which is used with the anti-diffusion technique is not oscillatory.
- The level set function (and also the VOF function) of liquid and gas phases is positive and negative, respectively.
- Flotsams and/or diffusion are only in cells with the distance of more than  $\delta_{ad}$  from the interface (i.e., cells which satisfy  $|\psi_{i,j}| > \delta_{ad}$ ) as shown in Fig. 1(a). Here,  $\delta_{ad}$  is the smoothing length of the interface of anti-diffusion. In this paper,  $\delta_{ad} = 1.5\Delta$  is used (this is equivalent to the interface thickness of  $3\Delta$ ) for the THINC/WLIC method and  $\delta_{ad} = \Delta$  for the VOF/WLIC method.

The outline of the anti-diffusion algorithm is shown in Figs. 1 and 2. In the proposed anti-diffusion algorithm, first, identify the flotsam and/or diffusion. As shown in Fig. 1(a), flotsams and/or diffusion are identified as  $C \neq 0$  on the gas phase side and  $C \neq 1$  on the liquid phase side and located at the distance of more than  $\delta_{ad}$  from the interface. Next, by using the unit normal vector to the interface calculated by the level set function, detected flotsam and/or diffusion are transported toward the interface to suppress flotsams and/or diffusion. As an important aspect of this proposed method, it is possible to guide  $C_{ad}$  to different positions. Utilizing this feature, four different types of anti-diffusion are proposed (which can be achieved by modifying parameters of the anti-diffusion algorithm). In type A, as shown in Fig. 2(a), flotsams and/or diffusion are moved inside the transition region of the interface but toward the outer side. In type B, as illustrated in Fig. 2(b), they are moved toward the center of the transition region of the interface. In type C, as shown in Fig. 2(c), they are moved beyond the center of the transition region of the interface. In type D, as depicted in Fig. 2(d), they are moved as far as possible to the opposite side within the transition region of the interface. This paper also discusses the differences between these types. In this paper, the CLSVOF method using the anti-diffusion algorithm will be referred to as CLSVOF-AD (CLSVOF with anti-diffusion) method.

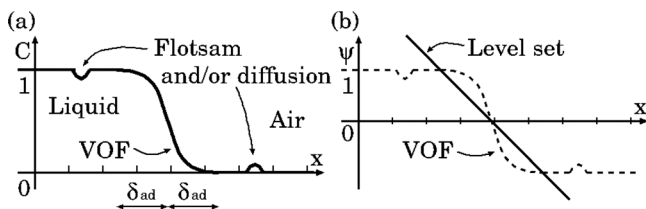


**FIG. 1.** Schematic figure of flotsams and/or diffusion in 1D (a).  $\delta_{ad}$  is the thickness of the transition region of anti-diffusion. (b) The relationship between the level set function and the VOF function.

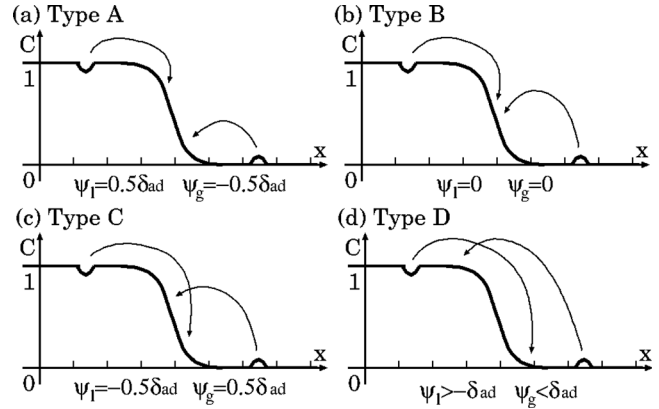


**FIG. 2.** Schematic figure of 1D anti-diffusion algorithms.  $\delta_{ad}$  is the thickness of the transition region of anti-diffusion. (a)–(c) correspond to type A, type B, and type C of the proposed method, respectively.

Here, we explain the details of the CLSVOF-AD method. The procedure is as follows:

1. Update the VOF function  $C$  using a VOF method (in this paper, the THINC/WLIC method or the VOF/WLIC method is used as the VOF method, but basically, any VOF method can be used).
2. Detect flotsams and/or diffusion in the gas phase. If the conditions  $C_{i,j} \neq 0$  and  $\psi_{i,j} < -\delta_{ad}$  are satisfied, the  $C_{i,j}$  is considered as a flotsam and/or diffusion.
3. Store these flotsams and/or diffusion into  $C_{ad,i,j} = C_{i,j}$  and reset the  $C_{i,j}$  to zero.
4. Transfer  $C_{ad,i,j}$  toward the transition region of the interface by solving the following advection equation:

$$\frac{\partial C_{ad}}{\partial t_{ad}} + \mathbf{n}_{ad} \cdot \nabla C_{ad} = 0 \tag{10}$$

with a conservative advection scheme, where  $t_{ad}$  is an artificial time for the advection equation, and  $\mathbf{n}_{ad}$  is modified surface normal which can be calculated by the level set function

$$\mathbf{n}_{ad} = \begin{cases} \frac{\nabla \psi}{|\nabla \psi|} & \text{if } \psi \leq \psi_g \\ -\frac{\nabla \psi}{|\nabla \psi|} & \text{if } \psi > \psi_g. \end{cases} \tag{11}$$

Equation (11) is the vector field to transfer  $C_{ad}$  to the nearest position on the contour line/surface of  $\psi = \psi_g$ . In this paper, to solve Eq. (10), we employ the fluid-in-cell (FLIC) method<sup>4</sup> (for some details of the FLIC method, see Appendix) and  $\Delta t_{ad} = 0.5\Delta / \max(|n_{ad,x}|, |n_{ad,y}|)$ . The advection equation is solved iteratively. In this calculation, flotsams and/or diffusion around the interface are just moved to contour line/surface of  $\psi = \psi_g$  within the transition region, so the number of iterations was set with some margin of safety as  $\text{int}(\frac{1.5(\delta_{ad} + \psi_g) + 2\Delta}{0.5\Delta})$ . To eliminate the possibility of numerical oscillations caused by the operation of the anti-diffusion, if  $C_{ad}$  reaches to cells of  $C_{i,j} = 1$  or  $C_{i,j} + C_{ad,i,j} = 1$ , we stop the reallocation process of the FLIC

- method to these cells of  $C_{i,j} = 1$  or  $C_{i,j} + C_{ad,i,j} = 1$ . Since  $\psi_g$  is a control parameter, the position of the contour/surface is adjustable. Therefore, in this paper, for types A, B, C, and D,  $\psi_g$  values of  $-0.5\delta_{ad}$ ,  $0$ ,  $0.5\delta_{ad}$ , and  $1.5\delta_{ad}$  (for type D, any value larger than  $\delta_{ad}$  can be used) are used (but user of the method can use any value). In type D, the intention is not to move  $C_{ad}$  to the contour of  $1.5\delta_{ad}$ , but rather to set a value greater than  $\delta_{ad}$  and use the above condition  $C_{i,j} = 1$  or  $C_{i,j} + C_{ad,i,j} = 1$  to move  $C_{ad}$  as far as possible toward the liquid phase side.
5. Redistribute transferred  $C_{ad}$  to  $C$ .  $C_{i,j} = C_{i,j} + C_{ad,i,j}$ . Processing of flotsams and/or diffusion in the gas phase is now complete.
  6. Detect flotsams and/or diffusion in the liquid phase. If the following conditions  $C_{i,j} \neq 1$  and  $\psi_{i,j} > \delta_{ad}$  are satisfied, the  $C_{i,j} - 1$  is considered as a flotsam and/or diffusion.
  7. Store these flotsams and/or diffusion into  $C_{ad,i,j} = C_{i,j} - 1$  and reset the  $C_{i,j}$  to one.
  8. Transfer  $C_{ad,i,j}$  toward the transition region of the interface by solving the advection equation (10) with the following  $\mathbf{n}_{ad}$ :

$$\mathbf{n}_{ad} = \begin{cases} \frac{\nabla\psi}{|\nabla\psi|} & \text{if } \psi \leq \psi_l \\ -\frac{\nabla\psi}{|\nabla\psi|} & \text{if } \psi > \psi_l. \end{cases} \quad (12)$$

- To eliminate the possibility of numerical oscillations caused by the operation of the anti-diffusion, if  $C_{ad}$  reaches to cells of  $C_{i,j} = 0$  or  $C_{i,j} + C_{ad,i,j} = 0$ , we stop the reallocation process of the FLIC method to these cells of  $C_{i,j} = 0$  or  $C_{i,j} + C_{ad,i,j} = 0$ . In this paper, for types A, B, C, and D,  $\psi_l$  values of  $0.5\delta_{ad}$ ,  $0$ ,  $-0.5\delta_{ad}$ , and  $-1.5\delta_{ad}$  (for type D, any value smaller than  $-\delta_{ad}$  can be used) are used.
9. Redistribute transferred  $C_{ad}$  to  $C$ .  $C_{i,j} = C_{i,j} + C_{ad,i,j}$ . Processing of flotsams and/or diffusion in the liquid phase is now complete.

The above is the procedure for the CLSVOF-AD method.

Although in this paper, we process flotsams and/or diffusion in the gas phase first, liquid phase second, it is also no problem to process flotsams and/or diffusion in the liquid phase first, gas phase second. These results are almost identical.

### C. Governing equations for free surface flows

In this paper, we consider incompressible flows and the following governing equations are used:

$$\int_{\Gamma_e} \mathbf{u} \cdot \mathbf{n} d\Gamma = 0, \quad (13)$$

$$\frac{\partial}{\partial t} \int_{\Omega_e} \mathbf{u} d\Omega + \int_{\Gamma_e} \mathbf{u}(\mathbf{u} \cdot \mathbf{n}) d\Gamma = -\frac{1}{\rho} \int_{\Gamma_e} p \mathbf{n} d\Gamma + \frac{1}{\rho} \int_{\Gamma_e} \boldsymbol{\tau} \cdot \mathbf{n} d\Gamma + \frac{\mathbf{F}_{sf}}{\rho}, \quad (14)$$

where  $\mathbf{n}$  is the outgoing normal for each control volume  $\Omega_e$  with its surface denoted by  $\Gamma_e$ ,  $\rho$  is the density,  $p$  is the pressure,  $\boldsymbol{\tau}$  is the viscous stress tensor, and  $\mathbf{F}_{sf}$  is the surface tension force. In this paper, we use the full variable Cartesian grid (FVCG) method<sup>41</sup> to solve these governing equations and the CIP-CSL2R (constrained interpolation profile-conservative semi-Lagrangian with second-order polynomial and rational functions) scheme<sup>40</sup> to solve the advection equation [although we use the FVCG method and the CIP-CSL2R scheme in this paper, any other fluid/advection equation solvers can be used such as ENO (essentially non-oscillatory),<sup>5</sup> WENO (weighted ENO) schemes,<sup>9,15,17</sup> other CIP-CSL schemes,<sup>13,14,20,32</sup> and VSIAM3-TM (volume/surface integrated average-based multi-moment method with temporary moment)<sup>1,31,42</sup>]. The surface tension force is calculated by the density scaled balanced continuum surface force model<sup>39,43</sup> with level set curvature correction.<sup>38</sup> For more details of the implementation of the free surface flow solver, see Refs. 37, 41, and 42.

In this paper, although the multi-moment method is employed in the fluid solver, it is not used for interface capturing (such as the VOF function and the level set function). Additionally, for the advection

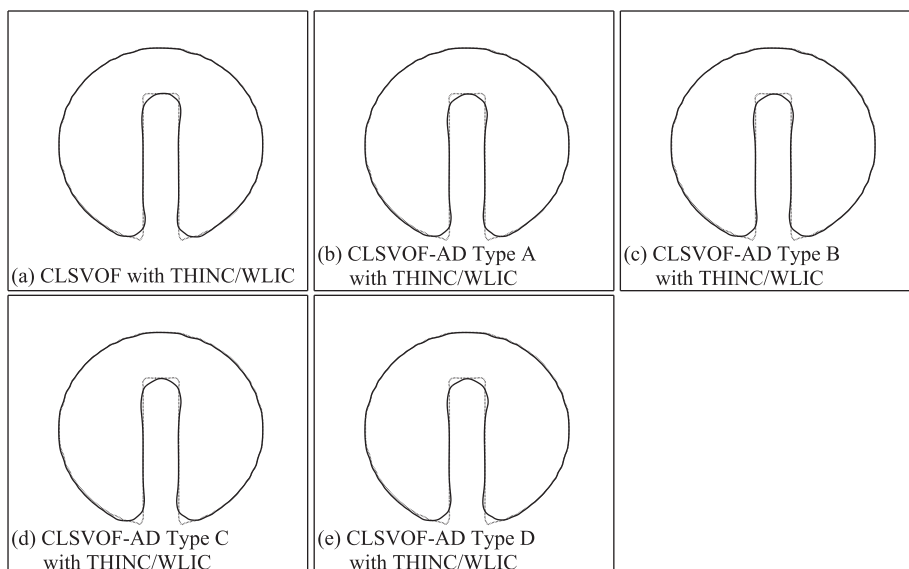


**FIG. 3.** Top views of numerical results of Zalesak problem after one revolution by the CLSVOF method without anti-diffusion (a) and the CLSVOF method type A (b), type B (c), type C (d), and type D (e) when the THINC/WLIC method is used as the VOF method. The solid and dot lines represent 0.5 contour lines of numerical results and exact solution, respectively. The Cartesian grid of  $100 \times 100$  was used.



**TABLE I.** Comparison of errors in Zalesak problem when the THINC/WLIC method is used as the VOF method. The Cartesian grid of  $100 \times 100$  is used.

Methods	L1 error
CLSVOF with THINC/WLIC	$3.93 \times 10^{-3}$
CLSVOF-AD type A with THINC/WLIC	$3.95 \times 10^{-3}$
CLSVOF-AD type B with THINC/WLIC	$3.93 \times 10^{-3}$
CLSVOF-AD type C with THINC/WLIC	$3.98 \times 10^{-3}$
CLSVOF-AD type D with THINC/WLIC	$4.08 \times 10^{-3}$

calculation of the VOF function, only the velocity components defined on a standard staggered grid are utilized.

### III. NUMERICAL RESULTS

We validated the proposed methods through Zalesak problem and single vortex flow test and comparisons with experiments of coalescence and separation of liquid droplets.<sup>2</sup>

#### A. Zalesak problem

Zalesak’s test problem<sup>44</sup> in which a notched circle is rotated is widely used as a test of scalar advection method. The initial condition is given by

$$C = \begin{cases} 1 & \text{if } \sqrt{(x - 0.5)^2 + (y - 0.75)^2} < 0.17 \\ & \text{and } (y > 0.85 \text{ or } |x - 0.5| > 0.03) \end{cases} \quad (15)$$

$$\mathbf{u}(x, y) = (y - 0.5, 0.5 - x). \quad (16)$$

The one revolution is completed with 628 time steps when Cartesian grids of  $100 \times 100$  are used. Figure 3 shows numerical results (top view) by the CLSVOF method without anti-diffusion (a) and the CLSVOF method type A (b), type B (c), type C (d), and type D (e) when the THINC/WLIC method is used as the VOF method. The

**TABLE II.** Comparison of errors in Zalesak problem when the VOF/WLIC method is used as the VOF method. The Cartesian grid of  $100 \times 100$  is used.

Methods	L1 error
CLSVOF with VOF/WLIC	$4.29 \times 10^{-3}$
CLSVOF-AD type A with VOF/WLIC	$4.40 \times 10^{-3}$
CLSVOF-AD type B with VOF/WLIC	$4.33 \times 10^{-3}$
CLSVOF-AD type C with VOF/WLIC	$4.56 \times 10^{-3}$
CLSVOF-AD type D with VOF/WLIC	$4.59 \times 10^{-3}$

solid and dot lines represent 0.5 contour lines of numerical results and exact solution, respectively. The Cartesian grid of  $100 \times 100$  was used. Table I shows the L1 errors. As shown in Fig. 3 and Table I, in this simple test, flotsams do not occur even without using the anti-diffusion, and all numerical results show a good agreement with the exact solution. This is because as can be understood from the algorithm, the anti-diffusion algorithm does not affect the VOF function in situations where flotsam and/or diffusion do not occur. The proposed method can almost fully maintain the high precision of interface capture, which is an advantage of the THINC/WLIC method, in situations where flotsams and/or diffusion do not occur. Table I shows that while the CLSVOF-AD type B reduces errors, in types A and C, errors are comparable to the CLSVOF method without using the anti-diffusion, and in type D, the error is slightly increased.

Figure 4 and Table II show the results when the VOF/WLIC method is used. The proposed anti-diffusion method functions similarly not only with the THINC/WLIC method but also with the VOF/WLIC method. For this test problem, the VOF/WLIC method is generally inferior to the THINC/WLIC method (it appears that the VOF/WLIC method is not proficient at handling sharp edges); however, it is evident that the anti-diffusion works similarly for the VOF/WLIC method. In this test problem, when the VOF/WLIC method is used, type A shows the best result, followed by types B–D. The error with type D becomes slightly larger

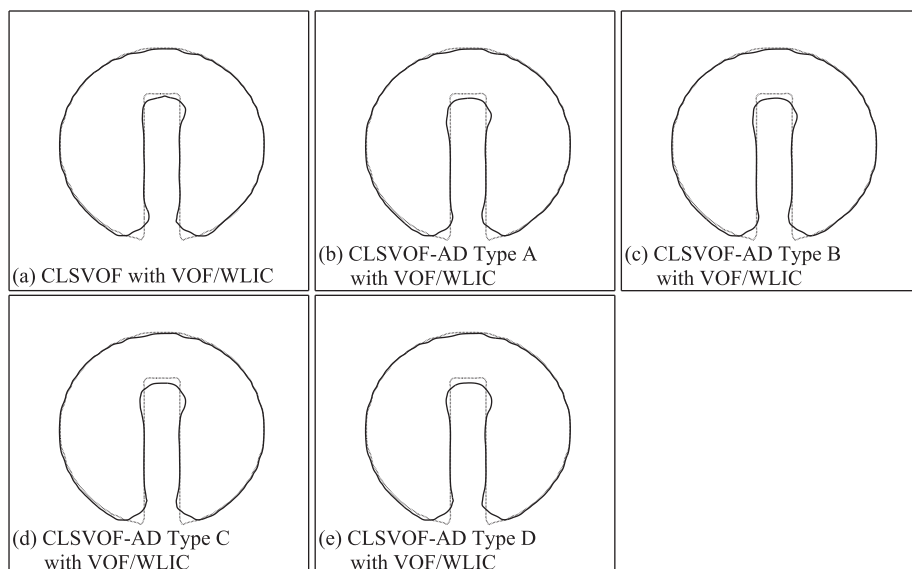


**FIG. 4.** Top views of numerical results of Zalesak problem after one revolution by the CLSVOF method without anti-diffusion (a) and the CLSVOF method type A (b), type B (c), type C (d), and type D (e) when the VOF/WLIC method is used as the VOF method. The solid and dot lines represent 0.5 contour lines of numerical results and exact solution, respectively. The Cartesian grid of  $100 \times 100$  was used.

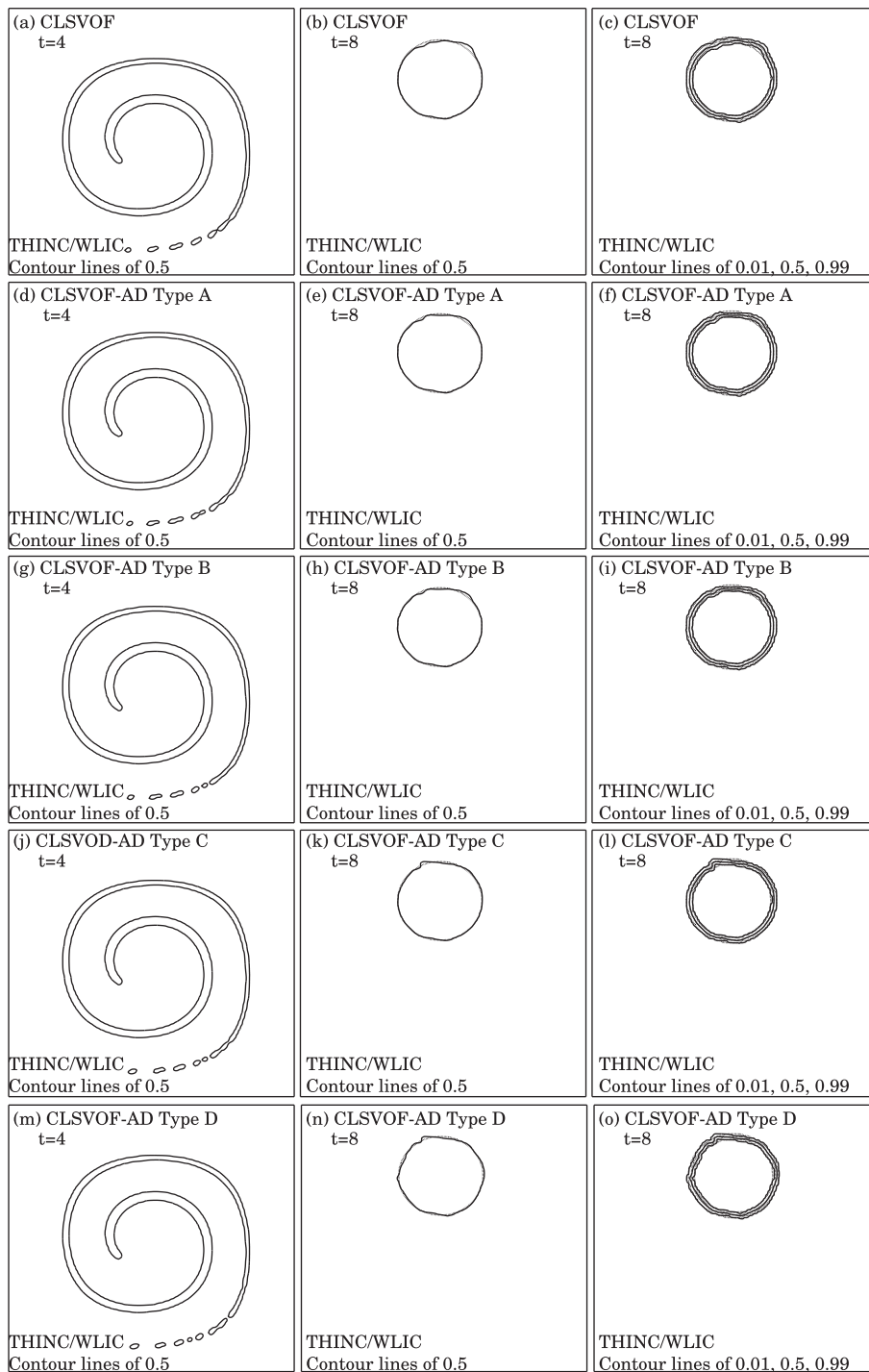


**FIG. 5.** Top views of numerical results of single vortex problem by the CLSVOF method without anti-diffusion (a)–(c) and the CLSVOF-AD method with anti-diffusion type A (d)–(f), type B (g)–(i), type C (j)–(l), and type D (m)–(o). The THINC/WLIC method was used as the VOF method. The solid and dot lines of (a and b), (d and e), (g and h), (j and k), and (m and n) represent 0.5 contour lines of numerical results and exact solution, respectively. The solid and dot lines of (c), (f), (i), (l), and (o) represent 0.01, 0.5, and 0.99 contour lines of numerical results and exact solution, respectively. The Cartesian grid of  $128 \times 128$  was used.

01 October 2024 13:03:21

than the CLSVOF method not using the anti-diffusion, similar to when the THINC/WLIC method is used.

Errors in the conservation of the VOF function were below  $10^{-14}$  (assuming the total initial VOF function is 1) in all cases in this test, indicating that the proposed anti-diffusion method do not

adversely affect conservation from these results. This is evident from the anti-diffusion algorithm, but the proposed method simply relocates flotsam and/or numerical diffusion to other cells, so theoretically, the proposed method does not cause conservation errors.

**TABLE III.** Comparison of errors in single vortex problem when the THINC/WLIC method was used as the VOF method. The Cartesian grids of  $32 \times 32$ ,  $64 \times 64$ , and  $128 \times 128$  were used.

Method	Grid size	L1 error	Order
CLSVOF with THINC/WLIC	$32 \times 32$	$4.77 \times 10^{-2}$	
	$64 \times 64$	$1.42 \times 10^{-2}$	1.74
	$128 \times 128$	$2.71 \times 10^{-3}$	2.40
CLSVOF-AD type A with THINC/WLIC	$32 \times 32$	$4.94 \times 10^{-2}$	
	$64 \times 64$	$1.24 \times 10^{-2}$	1.99
	$128 \times 128$	$2.11 \times 10^{-3}$	2.56
CLSVOF-AD type B with THINC/WLIC	$32 \times 32$	$5.18 \times 10^{-2}$	
	$64 \times 64$	$1.43 \times 10^{-2}$	1.86
	$128 \times 128$	$1.99 \times 10^{-3}$	2.84
CLSVOF-AD type C with THINC/WLIC	$32 \times 32$	$4.87 \times 10^{-2}$	
	$64 \times 64$	$1.49 \times 10^{-2}$	1.71
	$128 \times 128$	$2.16 \times 10^{-3}$	2.78
CLSVOF-AD type D with THINC/WLIC	$32 \times 32$	$4.71 \times 10^{-2}$	
	$64 \times 64$	$1.48 \times 10^{-2}$	1.67
	$128 \times 128$	$2.90 \times 10^{-3}$	2.35

## B. Single vortex flow test

To verify the proposed anti-diffusion technique in more complex scenario than Zalesak problem, we apply the proposed anti-diffusion technique to the single vortex problem.<sup>11,22</sup> The initial volume fraction distribution is a circle centered at (0.5, 0.75) with a radius of 0.15 on the computational domain  $[0, 1] \times [0, 1]$ . The velocity field is given by the stream function

$$\Psi = \frac{1}{\pi} \sin^2(\pi x) \cos^2(\pi y) \cos\left(\frac{\pi t}{T}\right). \quad (17)$$

The initial volume fraction is deformed by the velocity field, and it returns to its initial state at  $t = T$ .

Figure 5 shows the results by the CLSVOF method without anti-diffusion (a)–(c) and the CLSVOF-AD method type A (d)–(f), type B (g)–(i), type C (j)–(l), and type D (m)–(o), when the THINC/WLIC method was used as the VOF method.  $T = 8$  was used in this test. The solid and dot lines of Figs. 5(a) and 5(b), 5(d) and 5(e), 5(g) and 5(h), 5(j) and 5(k), and 5(m) and 5(n) represent 0.5 contour lines of numerical results and exact solution (initial condition), respectively. The solid and dot lines of (c), (f), (i), (l), and (o) represent 0.01, 0.5, and 0.99 contour lines of numerical results and exact solution, respectively. The Cartesian grid of  $128 \times 128$  was used. Table III shows  $L_1$  errors. In this test, although flotsam and/or diffusion do not occur significantly even without using the anti-diffusion, it can be observed from Fig. 5 and Table III, types A–C were able to improve the order of accuracy compared to when the anti-diffusion was not used. When using type D, the order of accuracy slightly decreases compared to when the anti-diffusion is not used.

Figure 6 and Table IV show the results by the VOF/WLIC method. When the anti-diffusion is not used, the VOF/WLIC method results in the formation of flotsams [as shown in Fig. 6(c)]. As shown in Table IV, when the anti-diffusion is utilized with types A–C, the order of accuracy is improved compared to it by the CLSVOF method

without anti-diffusion. Additionally, in the cases where types A–C were used, the results of the VOF/WLIC method outperformed those of the THINC/WLIC method. Although type A does not completely eliminate flotsam [as seen in Fig. 6(f)], types B–D make the VOF/WLIC method viable for practical numerical simulations. With type D, the order of accuracy slightly decreased compared to when the anti-diffusion is not used.

Here, we would like to consider why the differences by type occur. I believe there are primarily two causes of errors. The first is errors caused by the THINC and VOF methods (flotsams and diffusion), and the second is errors that occur when correcting these flotsams and diffusion (errors due to anti-diffusion). The results of these benchmark tests suggest that these two types of errors are competing. First, for type D, I believe that errors due to the THINC and VOF methods are sufficiently corrected. However, since the distance for moving the errors is longer than that of other types, errors due to anti-diffusion may become predominant, slightly reducing the order of accuracy. Next, looking at the results so far, type B seems to produce the best results. In type B, errors are moved to the center of the interface [Fig. 2(b)], which is considered the most mathematically rational type. Errors due to the THINC and VOF methods are appropriately corrected, and the distance for moving the errors is not excessively long. In type A, the correction of errors due to the THINC and VOF methods is slightly weaker, but because the distance for moving the errors is shorter, errors due to anti-diffusion are also minimized. Conversely, in type C, while errors due to the THINC and VOF methods are sufficiently corrected, the longer distance for moving the errors may result in a slight increase in errors due to anti-diffusion. I believe that these two types of errors are competing, leading to these results.

We also compared the numerical results using the proposed method with those obtained using other methods. First, we compared it with the conservative phase field methods, the conservative diffuse-interface (CDI) model, and the accurate conservative diffuse-interface (ACDI) model.<sup>8</sup> In Ref. 8, the direction of the velocity in the test is reversed, so we reversed the velocity field. Additionally, the resolution was set to  $256 \times 256$  to match the result in Ref. 8. The results of the comparison between CDI, ACDI, and CLSVOF-AD (type D, THINC/WLIC) are shown in Fig. 7. At  $t = 2$ , the CDI and ACDI methods show separations of the volume fraction at the edge, while the CLSVOF-AD method does not exhibit such separations. Furthermore, at  $t = 4$ , the results of the CDI and ACDI methods show a slight visible difference from the exact solution, but the result of the CLSVOF-AD method shows almost no visible error, indicating fewer errors. The quantitative comparison results are shown in Table V. For both the CLSVOF and CLSVOF-AD methods, the errors are approximately one-fourth that of the CDI method and about half that of the ACDI method. The difference in results will mainly be due to the differences in the advection solvers. The numerical diffusion using interface geometric reconstruction like VOF and THINC methods is significantly less than that of conventional advection solvers. When the numerical diffusion of the advection solver is large, the edges tend to round off and split easily during the advection calculation. Additionally, the diffusion term in the phase field model may also contribute to rounding the edges. On the other hand, the CLSVOF-AD method is designed to maintain the capability of the VOF and THINC methods as much as possible (only correcting errors and minimizing impact on the VOF



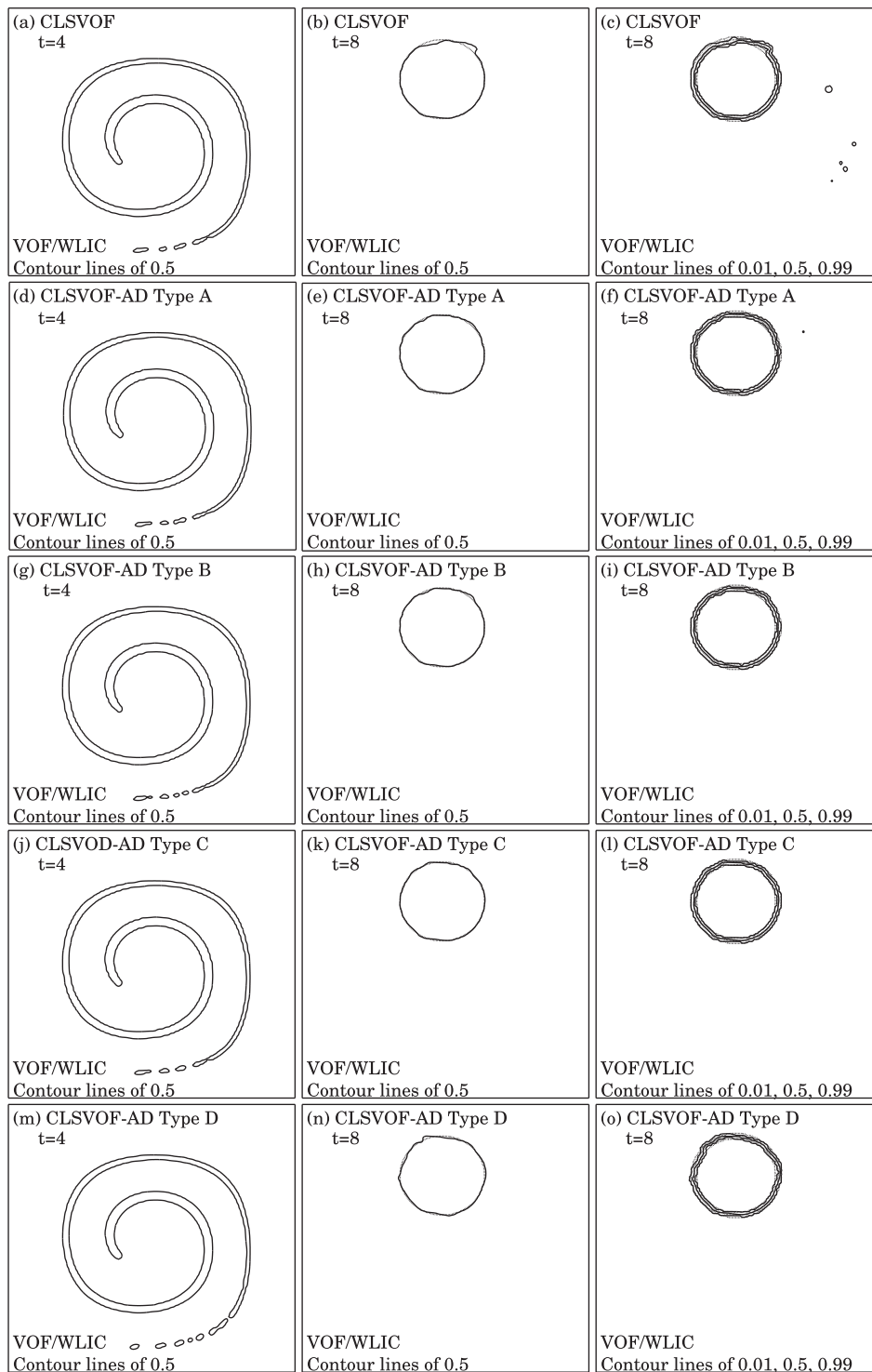


**FIG. 6.** Top views of numerical results of single vortex problem by the CLSVOF method without anti-diffusion (a)–(c) and the CLSVOF-AD method with anti-diffusion type A (d)–(f), type B (g)–(i), type C (j)–(l), and type D (m)–(o). The VOF/WLIC method was used as the VOF method. The solid and dot lines of (a and b), (d and e), (g and h), (j and k), and (m and n) represent 0.5 contour lines of numerical results and exact solution, respectively. The solid and dot lines of (c), (f), (i), (l), and (o) represent 0.01, 0.5, and 0.99 contour lines of numerical results and exact solution, respectively. The Cartesian grid of  $128 \times 128$  was used.

function, not solving the diffusion equation for the VOF function, etc.). Thus, the CLSVOF-AD method can suppress the issues of the VOF method (flotsam, slight numerical diffusion) while preserving its fundamental performance.

A comparison with the conservative level set method was also conducted.<sup>19</sup> The velocity field and initial conditions were set to be the same as in the paper.<sup>19</sup> Figure 8 shows the results of the conservative level set method (a)–(d) and the comparison with the CLSVOF-AD

**TABLE IV.** Comparison of errors in single vortex problem when the VOF/WLIC method was used as the VOF method. The Cartesian grids of  $32 \times 32$ ,  $64 \times 64$ , and  $128 \times 128$  were used.

Method	Grid size	L1 error	Order
CLSVOF with VOF/WLIC	$32 \times 32$	$5.56 \times 10^{-2}$	
	$64 \times 64$	$1.61 \times 10^{-2}$	1.79
	$128 \times 128$	$2.89 \times 10^{-3}$	2.47
CLSVOF-AD type A with VOF/WLIC	$32 \times 32$	$5.57 \times 10^{-2}$	
	$64 \times 64$	$1.47 \times 10^{-2}$	1.93
	$128 \times 128$	$1.91 \times 10^{-3}$	2.94
CLSVOF-AD type B with VOF/WLIC	$32 \times 32$	$6.61 \times 10^{-2}$	
	$64 \times 64$	$1.49 \times 10^{-2}$	2.15
	$128 \times 128$	$1.73 \times 10^{-3}$	3.11
CLSVOF-AD type C with VOF/WLIC	$32 \times 32$	$4.66 \times 10^{-2}$	
	$64 \times 64$	$1.56 \times 10^{-2}$	2.14
	$128 \times 128$	$1.65 \times 10^{-3}$	3.23
CLSVOF-AD type D with VOF/WLIC	$32 \times 32$	$5.13 \times 10^{-2}$	
	$64 \times 64$	$1.55 \times 10^{-2}$	1.74
	$128 \times 128$	$2.97 \times 10^{-3}$	2.39

method (e)–(h). In this comparison, the velocity field was set to twist in one direction only, and three contour lines (0.05, 0.5, and 0.95) were plotted. Similar to the results of the conservative phase field method mentioned above, the conservative level set method also showed a

**TABLE V.** Comparison of errors in single vortex problem when the VOF/WLIC method was used as the VOF method. The Cartesian grid of  $128 \times 128$  was used.

Method	L1 error
CDI	$1.95 \times 10^{-3}$
ACDI	$8.66 \times 10^{-4}$
CLSVOF with THINC/WLIC	$4.38 \times 10^{-4}$
CLSVOF-AD type A with THINC/WLIC	$4.35 \times 10^{-4}$
CLSVOF-AD type B with THINC/WLIC	$4.42 \times 10^{-4}$
CLSVOF-AD type C with THINC/WLIC	$4.50 \times 10^{-4}$
CLSVOF-AD type D with THINC/WLIC	$4.53 \times 10^{-4}$

tendency for edges and thin interface parts to split easily. Although similar splitting was observed with the CLSVOF-AD method, it was significantly less severe compared to the result of the conservative level set method. For a quantitative comparison with the conservative level set method, we compared the cases at  $T = 1$ . The error for the conservative level set method was  $7.2 \times 10^{-4}$ , while the error for the proposed method was  $3.35 \times 10^{-4}$ , approximately half.

**C. Coalescence and separation of liquid droplets**

We conducted 3D numerical simulations of free surface flows which include topology changes of liquid interfaces (coalescence and separation of liquid droplets)<sup>7</sup> to validate the CLSVOF-AD method in free surface flow applications.

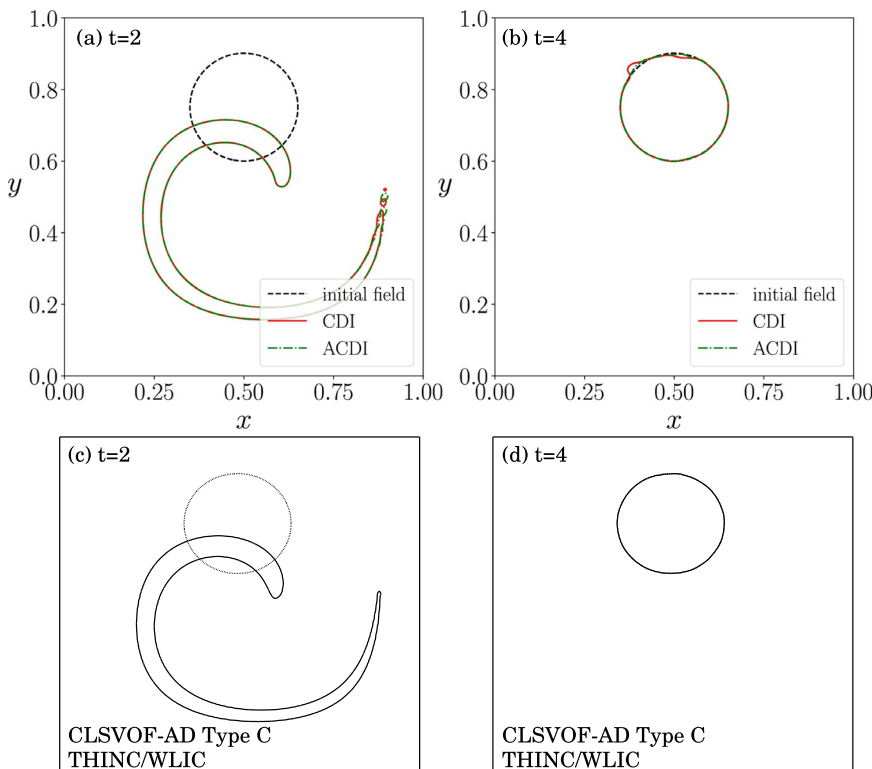


**FIG. 7.** Top views of numerical results of single vortex problem by CDI and ACDI (a) and (b) (reproduced with permission from S. S. Jain, *J. Comput. Phys.* **469**, 111529 (2022).<sup>8</sup> Copyright 2022 Elsevier) and the CLSVOF-AD method with anti-diffusion type C and the THINC/WLIC method (c) and (d). The lines represent 0.5 contour lines of numerical results and exact solution, respectively. The Cartesian grid of  $256 \times 256$  was used.

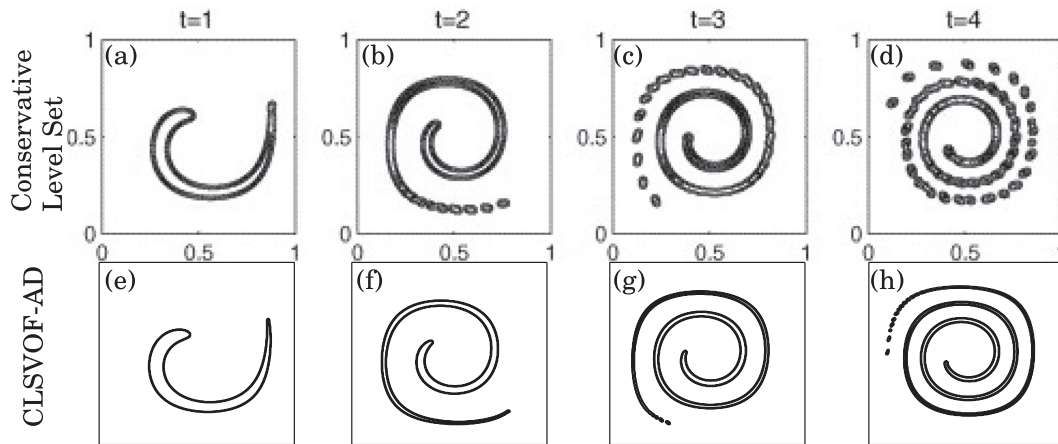


**FIG. 8.** Top views of numerical results of single vortex problem by the conservative level set method (a–d) (reproduced with permission from Olsson and Kreiss, *J. Comput. Phys.* **210**, 225–246 (2005).<sup>19</sup> Copyright 2005 Elsevier) and the CLSVOF-AD method with anti-diffusion type C and the THINC/WLIC method (e)–(h). The lines represent 0.05, 0.5, and 0.95 contour lines of numerical results and exact solution, respectively. The Cartesian grid of  $256 \times 256$  was used.

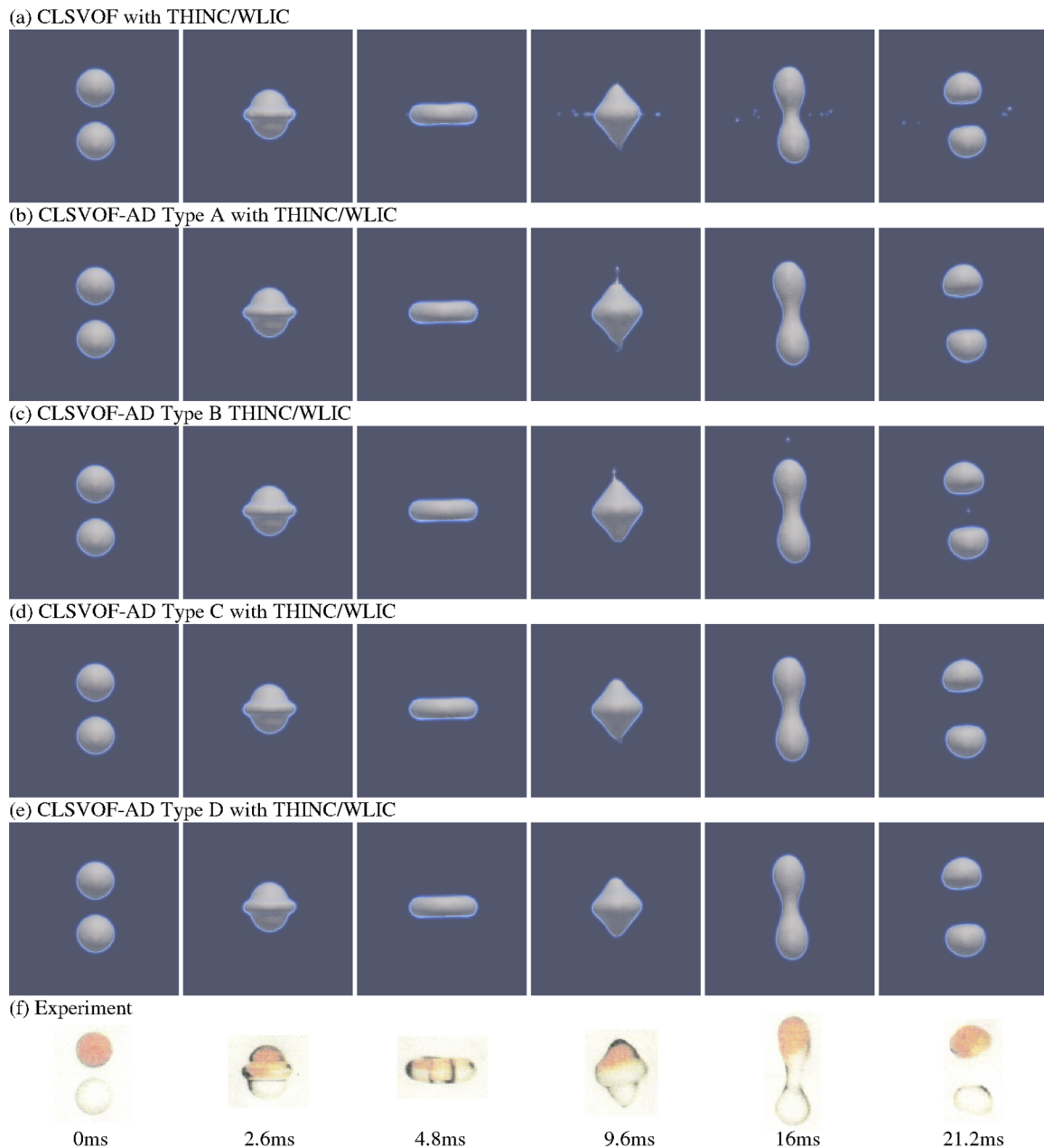
Figure 9 shows snapshots of the numerical results of  $We = 23$  by the CLSVOF method without anti-diffusion (a) and the CLSVOF-AD method type A (b), type B (c), type C (d), and type D (e) when the THINC/WLIC method was used as the VOF method. Figure 9(f) shows the corresponding experimental result.<sup>2</sup> Figures 9(a)–9(e) show liquid surfaces (0.5 contour of the VOF function) and also VOF function of less than 0.5. In these numerical simulations, quantitative parameters were used. The density ratio is 1.25:1000 (air:liquid). The mesh size  $\Delta = D/12$  was used, where  $D$  is the diameter of initial droplets. As shown in Fig. 9(a), when the anti-diffusion is not used, flotsams are generated. Flotsams are generated not only in the horizontal direction but also in the vertical direction as shown in Fig. 10(a). This result indicates that flotsams are more likely to occur when the gas–liquid interface retreats and when the advancing speed of the free surface slows down. Types A and B can prevent the generation of flotsams in the horizontal direction, but it cannot completely prevent the generation of flotsams in the vertical direction (however, it can achieve a certain level of suppression, such as delaying the generation). In Fig. 9(b) at 16 ms, vertical flotsams are not visible, so it may seem that type A has succeeded in suppressing vertical flotsams. However, this is because the flotsams have already flown out of the visualization domain. As shown in Fig. 10(b), type A cannot suppress vertical flotsams. Types C and D are effective in suppressing flotsams in this problem [Figs. 9(d) and 9(e)]. However, in type C, as visible at the bottom of the droplet in Fig. 9(d)  $t = 9.6$  ms, a flotsam appears to be on the verge of being generated, whereas in type D, this is not the case. From these results, it can be inferred that type D has the highest suppression capability of flotsams, followed by types C, B, and A in that order. This seems to be a reasonable result as type D moves flotsams furthest away from the interface, followed by types C, B, and A.

Figure 11 shows the numerical results of  $We = 23$  when the VOF/WLIC method was used as the VOF method. As shown in Fig. 11(a), using the VOF/WLIC method without anti-diffusion results in the generation of more flotsams than when using the THINC/WLIC method. When employing the VOF/WLIC method, the CLSVOF-AD method type A appears to produce a slight amount of flotsam, whereas types B–D are able to suppress the generation of

flotsams as shown in Figs. 11(b)–11(e). Upon careful observation of the results for types A and B at 9.6 ms in Fig. 11, it is apparent that flotsam is beginning to form at the top of the droplet (though it did not actually separate as a flotsam). However, when types C and D are used, such occurrences are not observed, suggesting that types C and D have a higher effectiveness in suppressing flotsams.

Figure 12 shows snapshots of the numerical results of  $We = 40$  by the CLSVOF method without anti-diffusion (a) and the CLSVOF-AD method type A (b), type B (c), type C (d), and type D (e), when the THINC/WLIC method was used as the VOF method. The corresponding experimental result is shown in Fig. 12(f).<sup>2</sup> As shown in Fig. 12(a), similar to the case of  $We = 23$ , when the anti-diffusion is not used, flotsams occur. However, as shown in Figs. 12(b)–12(e), the use of anti-diffusion effectively suppresses flotsams. There are slight differences in the results at  $t = 25.6$  ms, but as shown in Fig. 13, ultimately, all types of CLSVOF-AD methods completely separate into only two liquid droplets without flotsams. In situations where there are relatively few flotsams (there is not much retreat of gas–liquid interfaces, etc.), any type could suppress flotsams.

Figure 14 shows the numerical results of  $We = 40$  by the CLSVOF method without anti-diffusion (a) and the CLSVOF-AD method type A (b), type B (c), type C (d), and type D (e), when the VOF/WLIC method was used as the VOF method. Using the VOF/WLIC method without applying the anti-diffusion, more flotsams were generated compared to the THINC/WLIC method, and the droplets ultimately did not separate [Fig. 14(a)]. However, when the anti-diffusion was applied, flotsams could be suppressed by all types of the CLSVOF-AD method, and droplet separation was reproduced. In the 25.6 ms snapshot of type A, something resembling flotsam can be observed between the droplets. It will be more natural to consider these as small droplets left behind when the main droplets separated, rather than as flotsam, as they are eventually absorbed by the two larger droplets. Slight differences can be observed at 23.2 ms, but ultimately, the droplets separate into two. The VOF/WLIC method on its own is inferior to the THINC/WLIC method, and in the example shown in Fig. 14(a), the droplet did not split, making it a less practical method. However, by combining the VOF/WLIC method with the



**FIG. 9.** Numerical results of two droplet coalescence and separation of  $We = 23$  by the CLSVOF method without anti-diffusion (a) and the CLSVOF-AD method type A (b), type B (c), type C (d), and type D (e). (f) The corresponding experiment (reproduced with permission from Ashgriz and Poo, *J. Fluid Mech.* **221**, 183–204 (1990).<sup>2</sup> Copyright 1990 Cambridge University Press). (a)–(e) Liquid surfaces (0.5 contour of the VOF function) and also VOF function of less than 0.5. The THINC/WLIC method was used as the VOF method. The mesh size is  $\Delta = D/12$ .

anti-diffusion technique, it was found to be a sufficiently practical interface capturing method.

To examine the conservation of the VOF function when the proposed anti-diffusion technique is applied to actual fluid problems, we investigated the conservation using the examples shown in Fig. 12. As indicated in Fig. 15, there was no impact on the conservation due to

the proposed anti-diffusion technique. No conservation errors occurred in all cases in this section. This is because the proposed anti-diffusion technique simply relocates flotsams and/or diffusion to other cells, thereby ensuring no compromise in conservation.

To investigate the impact of the proposed method on computation time, we compared calculation times of the CLSVOF method

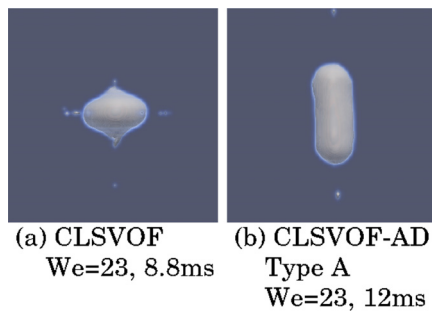


**FIG. 10.** (a) A numerical result of two droplet coalescence and separation of  $We = 23$  by the CLSVOF method without anti-diffusion at  $t = 8.8$  ms. (b) A numerical result of  $We = 23$  by the CLSVOF-AD method type A at  $t = 12$  ms. The THINC/WLIC method was used as the VOF method.

and CLSVOF-AD method using the case with  $We = 40$ . The results are shown in Table VI. The times in the table are normalized with the computation time by the CLSVOF method set to 1.

As shown in Table VI, the increase in computation time due to the CLSVOF-AD method is approximately 0.5%–2% in this example. The calculation time increases more in the THINC method case than in the VOF method case. This is because the movement distance of flotsam/diffusion is longer in the THINC method case, resulting in more frequent calculations of the advection equation. Additionally, the calculation time increases from type A to type D, which is also due to the increasing movement distance of flotsam/diffusion from type A to type D.

#### D. Droplet splashing

To verify the proposed method with a more challenging problem, we conducted numerical simulations of a prompt splashing using the

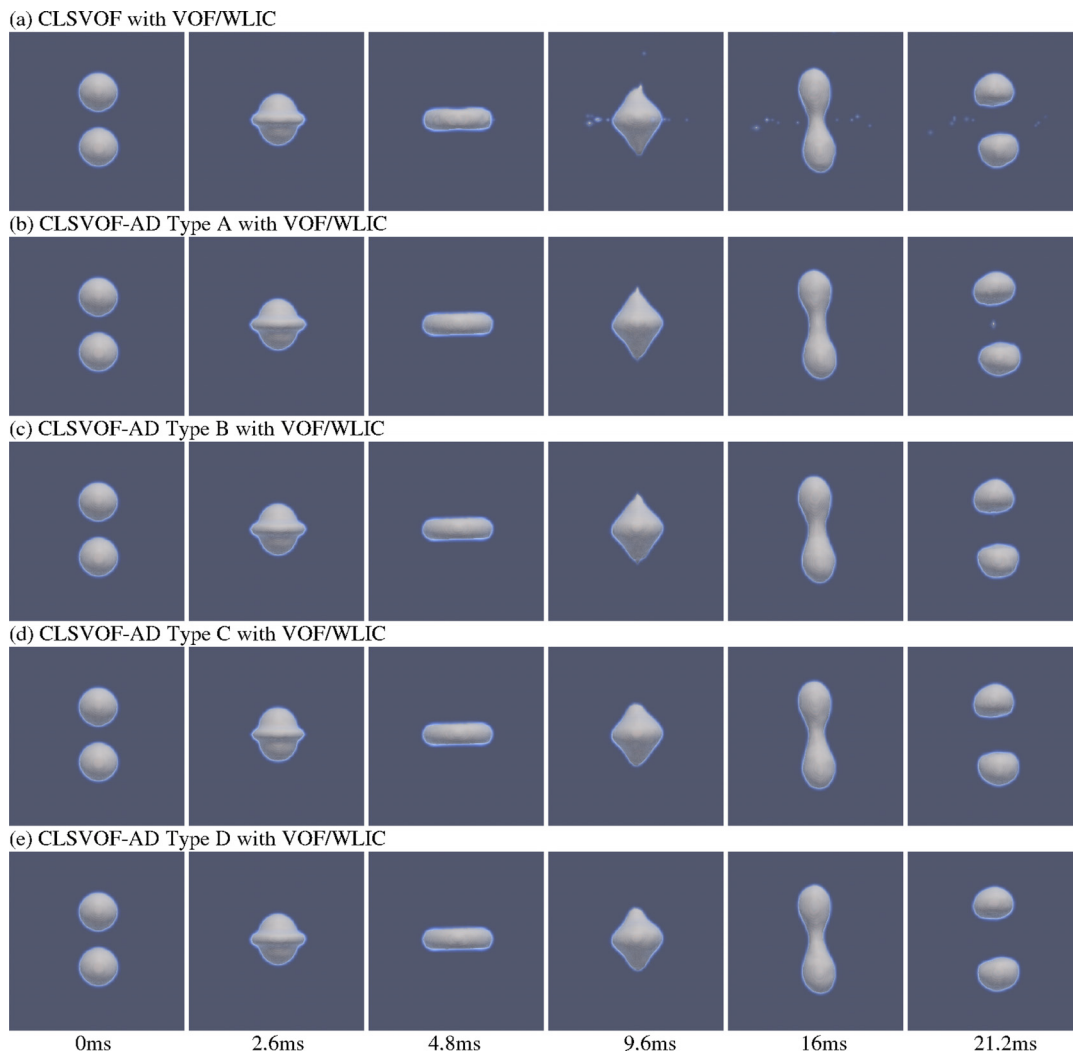


**FIG. 11.** Numerical results of two droplet coalescence and separation of  $We = 23$  by the CLSVOF method without anti-diffusion (a) and the CLSVOF-AD method type A (b), type B (c), type C (d), and type D (e). (a)–(e) Liquid surfaces (0.5 contour of the VOF function) and also VOF function of less than 0.5. The THINC/WLIC method was used as the VOF method. The mesh size is  $\Delta = D/12$ .



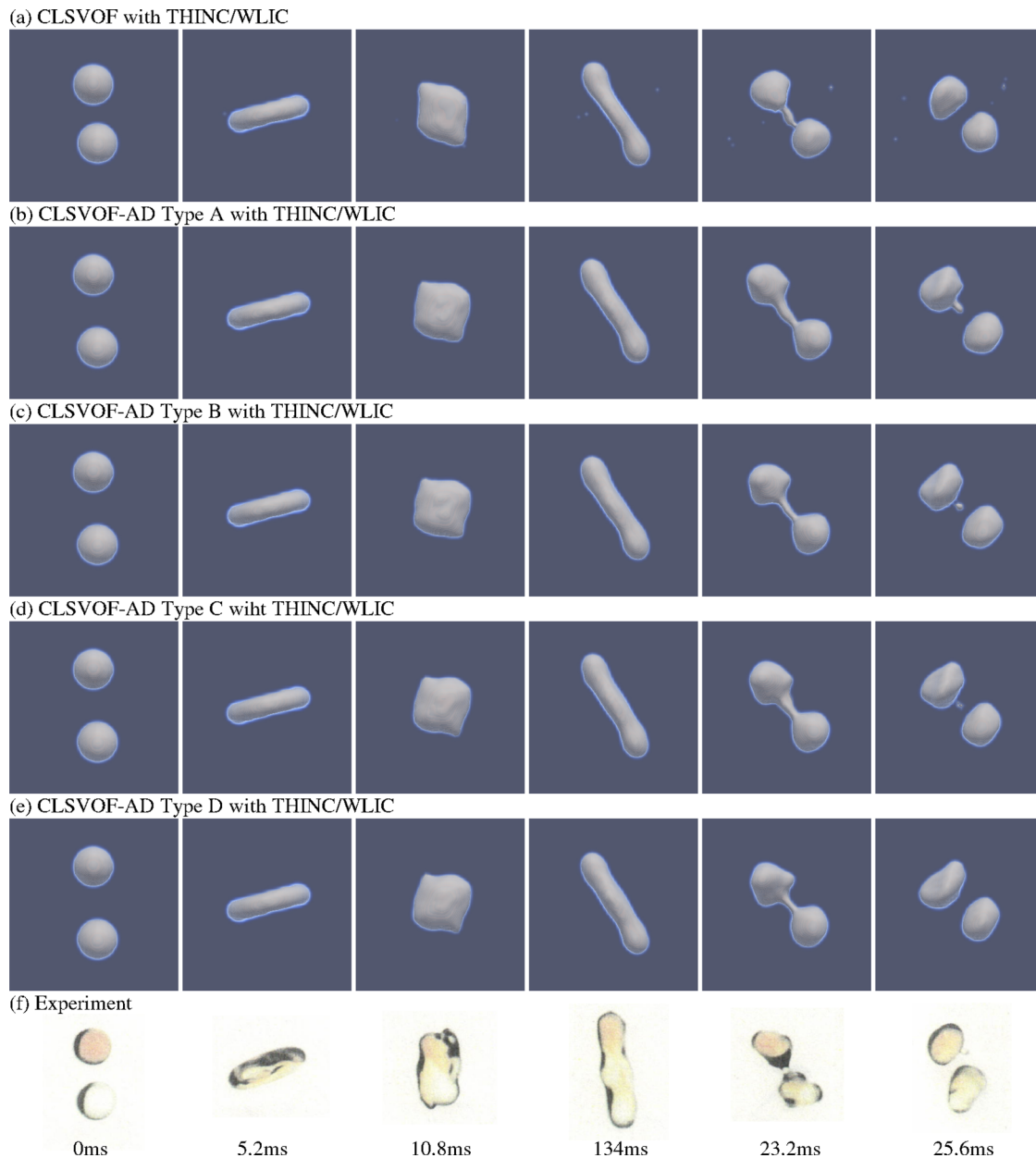


**FIG. 12.** Numerical results of two droplet coalescence and separation of  $We = 40$  by the FVCG method without anti-diffusion (a) and the CLSVOF-AD method type A (b), type B (c), type C (d), and type D (e). (f) The corresponding experiment (reproduced with permission from Ashgriz and Poo, *J. Fluid Mech.* **221**, 183–204 (1990).<sup>2</sup> Copyright 1990 Cambridge University Press). (a)–(e) Liquid surfaces (0.5 contour of the VOF function) and also VOF function of less than 0.5. The VOF/WLIC method was used as the VOF method. The mesh size is  $\Delta = D/12$ .

CLSVOF method and the CLSVOF-AD method and compared these numerical results. The THINC/WLIC method was used as the VOF method, and type D was used due to the complexity of the problem. The corresponding experimental result can be found in Ref. 28. In the comparison, quantitative parameters, the densities  $\rho_{liquid} = 1000 \text{ kg/m}^3$ ,  $\rho_{air} = 1.25 \text{ kg/m}^3$ , viscosities  $\mu_{liquid} = 1.0 \times 10^{-3} \text{ Pa s}$ ,  $\mu_{air} = 1.82 \times 10^{-5} \text{ Pa s}$ , surface tension  $\sigma = 7.2 \times 10^{-2} \text{ N/m}$ , gravity

$9.8 \text{ m/s}^2$ , initial droplet diameter  $D = 1.86 \text{ mm}$ , impact speed  $2.98 \text{ m/s}$ , and the equilibrium contact angle  $163^\circ$ , are used. A Cartesian grid of  $224 \times 224 \times 48$  and  $\Delta = D_{splash}/46$  is used, where  $D_{splash}$  is the diameter of the initial droplet. Figure 16 shows the numerical result. The CLSVOF method captures the splash, but flotsams and diffusion of the VOF function are observed [Fig. 16(a)]. On the other hand, the CLSVOF-AD method captures the splash as well as the CLSVOF

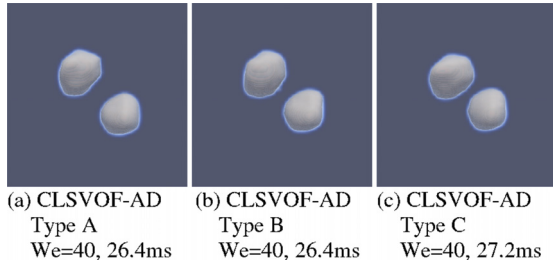


**FIG. 13.** (a)–(c) Numerical results of two droplet coalescence and separation of  $We = 40$  by the CLSVOF-AD method type A at  $t = 26.4$  ms, type B at  $t = 26.4$  ms, and type C at  $t = 27.2$  ms, respectively. The THINC/WLIC method was used as the VOF method.

method while suppressing the flotsams and diffusion of the VOF function [Fig. 16(b)].

**IV. SUMMARY**

In this paper, we proposed the CLSVOF-AD method to suppress flotsams and/or diffusion in the CLSVOF method. The proposed method can effectively suppress flotsams and/or diffusion while maintaining the reproducibility of fluid phenomena (or the reproducibility is improved) and preserving conservation laws. The CLSVOF-AD method works with both the THINC method and the VOF method. In this paper, four different types of the CLSVOF-AD method (types A–D) were considered. Types A and B demonstrate better performance in the simple benchmark tests (Zalesak problem and single vortex flow test). However, the effectiveness of suppressing flotsams in

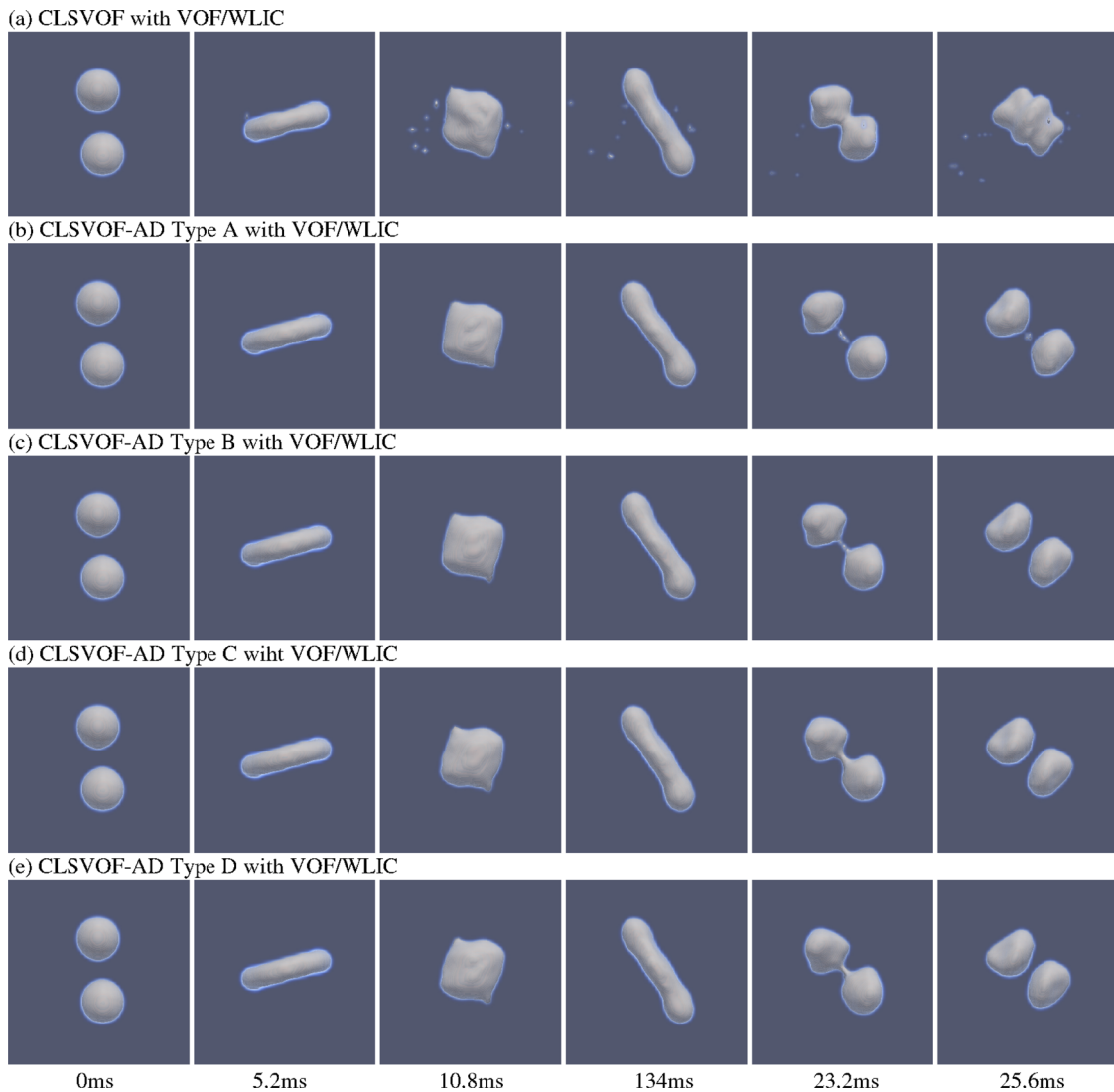


**FIG. 14.** Numerical results of two droplet coalescence and separation of  $We = 40$  by the FVCG method without anti-diffusion (a) and the CLSVOF-AD method type A (b), type B (c), type C (d), and type D (e). (a)–(e) Liquid surfaces (0.5 contour of the VOF function) and also VOF function of less than 0.5. The VOF/WLIC method was used as the VOF method. The mesh size is  $\Delta = D/12$ .

01 October 2024 13:03:21

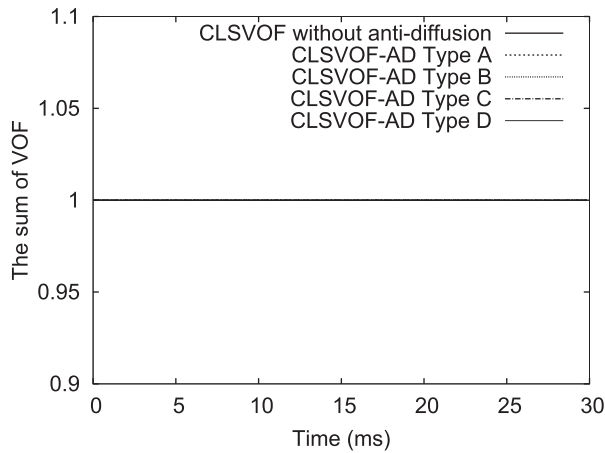


**FIG. 15.** The conservation test of the numerical simulations of Fig. 12 by the CLSVOF method without anti-diffusion and the CLSVOF-AD methods type A, type B, type C, and type D. The initial sum of VOF function is normalized as 1.

**TABLE VI.** Comparison of computation times for the case with  $We = 40$ . The Cartesian grid of  $64 \times 64 \times 64$  was used.

Method	Time
CLSVOF with THINC/WLIC	1
CLSVOF-AD type A with THINC/WLIC	1.017
CLSVOF-AD type B with THINC/WLIC	1.018
CLSVOF-AD type C with THINC/WLIC	1.020
CLSVOF-AD type D with THINC/WLIC	1.022
CLSVOF with VOF/WLIC	1
CLSVOF-AD type A with VOF/WLIC	1.005
CLSVOF-AD type B with VOF/WLIC	1.006
CLSVOF-AD type C with VOF/WLIC	1.011
CLSVOF-AD type D with VOF/WLIC	1.013

actual fluid problems is weaker compared to types C and D. While type D shows relatively poor performance in these simple benchmark tests, it exhibits the highest effectiveness in suppressing flotsams in actual fluid simulations. Type C has performance that is intermediate between types A and B, and type D. The choice of CLSVOF-AD method type depends on the situation, where types A or B is suitable when flotsams and/or diffusion are not prevalent, and types C or D is recommended for computational targets prone to flotsams (although this paper categorizes them as types A–D for convenience, in reality, the control parameters ( $\psi_g$  and  $\psi_l$ ) can be continuously adjusted, allowing users to use their preferred control parameters).

**ACKNOWLEDGMENTS**

This research was supported in part by FLEXIS and IROHMS, which are part-funded by the European Regional Development Fund (ERDF), through the Welsh Government. The numerical simulations were partially conducted on computers at Yukawa Institute of Theoretical Physics in Kyoto University and at HPC Wales. We acknowledge the support of the Supercomputing Wales project, which is part-funded by the European Regional Development Fund (ERDF) via Welsh Government.

**AUTHOR DECLARATIONS**

**Conflict of Interest**

The author has no conflicts to disclose.

**Author Contributions**

**Kensuke Yokoi:** Conceptualization (lead); Data curation (lead); Formal analysis (lead); Funding acquisition (lead); Investigation (lead); Methodology (lead); Project administration (lead); Resources (lead); Software (lead); Validation (lead); Visualization (lead); Writing – original draft (lead); Writing – review & editing (lead).

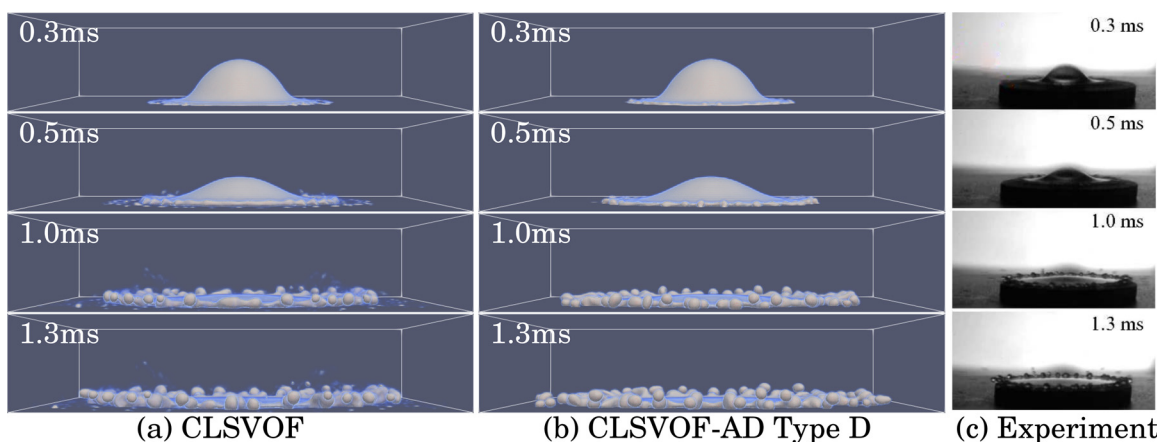


**FIG. 16.** Numerical results of droplet splashing by the CLSVOF method with the THINC/WLIC method (a), the CLSVOF-AD method (type D) with the THINC/WLIC method (b), and the corresponding experimental result (c) (reproduced with permission from Tsai *et al.*, *Langmuir* **25**(20), 12293–12298 (2009).<sup>28</sup> Copyright 2009 American Chemical Society). (a) and (b) Liquid surfaces (0.5 contour of the VOF function) and also VOF function of less than 0.5. A distilled water droplet of 1.86 (mm) impacts onto a superhydrophobic substrate (the equilibrium angle is  $163^\circ$ ). The droplet impact speed is 2.98 (m/s). A Cartesian grid of  $224 \times 224 \times 48$  is used.

01 October 2024 13:03:21

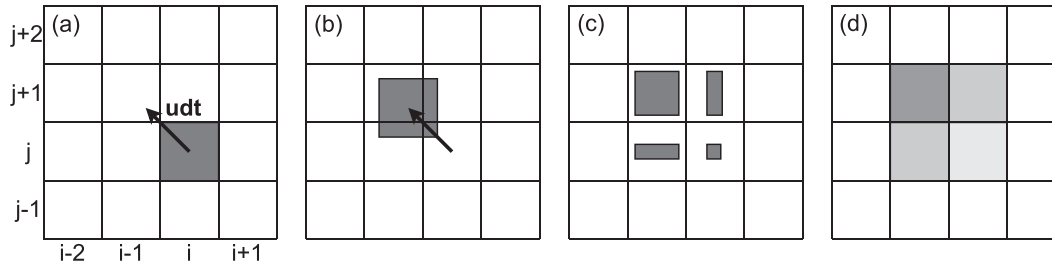


FIG. 17. Schematic figure of the FLIC method.

DATA AVAILABILITY

The data that supports the findings of this study are available within the article.

APPENDIX: FLUID-IN-CELL (FLIC)

The FLIC method is a simple conservative advection scheme. A schematic figure of 2D FLIC advection process is shown in Fig. 17.

Now, let us focus on the quantity  $f_{i,j}$  in the cell  $(i, j)$  and how the quantity is transferred. First,  $f_{i,j}$  is transported like a particle according to the velocity  $\mathbf{u}_{i,j} = (u_{i,j}, v_{i,j})$  as shown in Figs. 17(a) and 17(b) (In the proposed anti-diffusion algorithms, the transported quantity is going to be  $C_{ad}$  instead of  $f$  and the velocity is going to be  $\mathbf{n}_{ad}$  instead of  $\mathbf{u}$ ). The quantity  $f_{i,j}$  is distributed into four cells as shown in Figs. 17(c) and 17(d). The mathematical formula is

$$\Delta f_{i,j}^{n+1} = f_{i,j}^n(dx - |u_{i,j}|dt)(dy - |v_{i,j}|dt), \tag{A1}$$

$$\Delta f_{i-1,j}^{n+1} = f_{i,j}^n|u_{i,j}|dt(dy - |v_{i,j}|dt), \tag{A2}$$

$$\Delta f_{i,j+1}^{n+1} = f_{i,j}^n(dx - |u_{i,j}|dt)|v_{i,j}|dt, \tag{A3}$$

$$\Delta f_{i-1,j+1}^{n+1} = f_{i,j}^n|u_{i,j}|dt|v_{i,j}|dt. \tag{A4}$$

The FLIC method is easy to implement (not only 2D but also 3D) and robust.

REFERENCES

<sup>1</sup>Al-Mosallam, M. and Yokoi, K., “Efficient implementation of volume/surface integrated average-based multi-moment method,” *Int. J. Comput. Methods* **14**(2), 1750010 (2017).  
<sup>2</sup>Ashgriz, N. and Poo, J. Y., “Coalescence and separation in binary collisions of liquid drops,” *J. Fluid Mech.* **221**, 183–204 (1990).  
<sup>3</sup>Chiu, P.-H. and Lin, Y.-T., “A conservative phase field method for solving incompressible two-phase flows,” *J. Comput. Phys.* **230**(1), 185–204 (2011).  
<sup>4</sup>Gentry, R. A., Martin, R. E., and Daly, B. J., “An Eulerian differencing method for unsteady compressible flow problems,” *J. Comput. Phys.* **1**(1), 87–118 (1966).  
<sup>5</sup>Harten, A., Engquist, B., Osher, S., and Chakravarthy, S. R., “Uniformly high order accurate essentially non-oscillatory schemes, III,” *J. Comput. Phys.* **71**(2), 231–303 (1987).  
<sup>6</sup>Hirt, C. and Nichols, B., “Volume of fluid (VOF) method for the dynamics of free boundaries,” *J. Comput. Phys.* **39**(1), 201–225 (1981).  
<sup>7</sup>Ii, S., Sugiyama, K., Takeuchi, S., Takagi, S., Matsumoto, Y., and Xiao, F., “An interface capturing method with a continuous function: The THINC method with multi-dimensional reconstruction,” *J. Comput. Phys.* **231**(5), 2328–2358 (2012).

<sup>8</sup>Jain, S. S., “Accurate conservative phase-field method for simulation of two-phase flows,” *J. Comput. Phys.* **469**, 111529 (2022).  
<sup>9</sup>Jiang, G.-S. and Shu, C.-W., “Efficient implementation of weighted ENO schemes,” *J. Comput. Phys.* **126**(1), 202–228 (1996).  
<sup>10</sup>Kim, J., “A continuous surface tension force formulation for diffuse-interface models,” *J. Comput. Phys.* **204**(2), 784–804 (2005).  
<sup>11</sup>LeVeque, R. J., “High-resolution conservative algorithms for advection in incompressible flow,” *SIAM J. Numer. Anal.* **33**(2), 627–665 (1996).  
<sup>12</sup>Li, J., “Calcul d’interface affine par morceaux,” *C. R. Acad. Sci.* **320**(8), 391–396 (1995).  
<sup>13</sup>Li, Q., Omar, S., Deng, X., and Yokoi, K., “Constrained interpolation profile conservative semi-Lagrangian scheme based on third-order polynomial functions and essentially non-oscillatory (CIP-CSL3ENO) scheme,” *Commun. Comput. Phys.* **22**(3), 765–788 (2017).  
<sup>14</sup>Q. Li, J. Xia, K. Yokoi, and S. Omar, “Boundary variation diminished conservative semi-Lagrangian method for both compressible and incompressible flows,” *Phys. Fluids* **33**(11), 117114 (2021).  
<sup>15</sup>Li, Q., Yokoi, K., Xie, Z., Omar, S., and Xue, J., “A fifth-order high-resolution shock-capturing scheme based on modified weighted essentially non-oscillatory method and boundary variation diminishing framework for compressible flows and compressible two-phase flows,” *Phys. Fluids* **33**(5), 056104 (2021).  
<sup>16</sup>Lin, J. and Yao, H.-D., “Modified Magnus effect and vortex modes of rotating cylinder due to interaction with free surface in two-phase flow,” *Phys. Fluids* **35**(12), 123614 (2023).  
<sup>17</sup>Liu, X.-D., Osher, S., and Chan, T., “Weighted essentially non-oscillatory schemes,” *J. Comput. Phys.* **115**(1), 200–212 (1994).  
<sup>18</sup>Matsushita, S. and Aoki, T., “A weakly compressible scheme with a diffuse-interface method for low Mach number two-phase flows,” *J. Comput. Phys.* **376**, 838–862 (2019).  
<sup>19</sup>Olsson, E. and Kreiss, G., “A conservative level set method for two phase flow,” *J. Comput. Phys.* **210**(1), 225–246 (2005).  
<sup>20</sup>Onodera, N., Aoki, T., and Yokoi, K., “A fully conservative high-order upwind multi-moment method using moments in both upwind and downwind cells,” *Numer. Methods Fluids* **82**(8), 493–511 (2016).  
<sup>21</sup>Osher, S. and Sethian, J. A., “Fronts propagating with curvature-dependent speed: Algorithms based on Hamilton-Jacobi formulations,” *J. Comput. Phys.* **79**(1), 12–49 (1988).  
<sup>22</sup>Rider, W. J. and Kothe, D. B., “Reconstructing volume tracking,” *J. Comput. Phys.* **141**(2), 112–152 (1998).  
<sup>23</sup>Rudman, M., “Volume-tracking methods for interfacial flow calculations,” *Int. J. Numer. Methods Fluids* **24**, 671–691 (1998).  
<sup>24</sup>Scardovelli, R. and Zaleski, S., “Direct numerical simulation of free-surface and interfacial flow,” *Annu. Rev. Fluid Mech.* **31**(1), 567–603 (1999).  
<sup>25</sup>Sussman, M. and Puckett, E. G., “A coupled level set and volume-of-fluid method for computing 3D and axisymmetric incompressible two-phase flows,” *J. Comput. Phys.* **162**(2), 301–337 (2000).  
<sup>26</sup>Sussman, M., Smereka, P., and Osher, S., “A level set approach for computing solutions to incompressible two-phase flow,” *J. Comput. Phys.* **114**(1), 146–159 (1994).  
<sup>27</sup>Tryggvason, G., Scardovelli, R., and Zaleski, S., *Direct Numerical Simulations of Gas-Liquid Multiphase Flows* (Cambridge University Press, 2011).

01 October 2024 13:03:21

- <sup>28</sup>Tsai, P., Pacheco, S., Pirat, C., Lefferts, L., and Lohse, D., “Drop impact upon micro- and nanostructured superhydrophobic surfaces,” *Langmuir* **25**(20), 12293–12298 (2009).
- <sup>29</sup>Wang, S.-J., Shi, Z.-H., Yao, T.-L., Li, W.-F., and Lin, Q.-G., “Experimental and numerical study of liquid film by jet impingement: Based on contact angle model,” *Phys. Fluids* **35**(8), 085104 (2023).
- <sup>30</sup>Xiao, F., Honma, Y., and Kono, T., “A simple algebraic interface capturing scheme using hyperbolic tangent function,” *Numer. Methods Fluids* **48**(9), 1023–1040 (2005).
- <sup>31</sup>Xiao, F., Ikebata, A., and Hasegawa, T., “Numerical simulations of free-interface fluids by a multi-integrated moment method,” *Comput. Struct.* **83**(6–7), 409–423 (2005).
- <sup>32</sup>Xiao, F., Yabe, T., Peng, X., and Kobayashi, H., “Conservative and oscillation-less atmospheric transport schemes based on rational functions,” *J. Geophys. Res.* **107**(D22), ACL 2-1–ACL 2-11, <https://doi.org/10.1029/2001JD001532> (2002).
- <sup>33</sup>Xiao, M., Yang, G., Huang, Y., and Wu, J., “Evaluation of different interface-capturing methods for cryogenic two-phase flows under microgravity,” *Phys. Fluids* **34**(11), 112124 (2022).
- <sup>34</sup>Xiong, Y., Xie, B., and Xiao, F., “A coupled level-set and tangent of hyperbola interface capturing (THINC) scheme with a single-step time integration for incompressible flows,” *Phys. Fluids* **35**(11), 112102 (2023).
- <sup>35</sup>Yokoi, K., “Numerical method for complex moving boundary problems in a Cartesian fixed grid,” *Phys. Rev. E* **65**, 055701 (2002).
- <sup>36</sup>Yokoi, K., “Efficient implementation of THINC scheme: A simple and practical smoothed VOF algorithm,” *J. Comput. Phys.* **226**(2), 1985–2002 (2007).
- <sup>37</sup>Yokoi, K., “A numerical method for free-surface flows and its application to droplet impact on a thin liquid layer,” *J. Sci. Comput.* **35**(2), 372–396 (2008).
- <sup>38</sup>Yokoi, K., “A practical numerical framework for free surface flows based on CLSVOF method, multi-moment methods and density-scaled CSF model: Numerical simulations of droplet splashing,” *J. Comput. Phys.* **232**(1), 252–271 (2013).
- <sup>39</sup>Yokoi, K., “A density-scaled continuum surface force model within a balanced force formulation,” *J. Comput. Phys.* **278**, 221–228 (2014).
- <sup>40</sup>Yokoi, K., “Third-order less oscillatory and less diffusive compact stencil-based upwind schemes, and their applications to incompressible flows and free surface flows,” *Phys. Fluids* **34**(11), 112104 (2022).
- <sup>41</sup>Yokoi, K., “Full-variable Cartesian grid method for incompressible and multi-phase flows,” *J. Comput. Phys.* **500**, 112749 (2024).
- <sup>42</sup>Yokoi, K., Furuichi, M., and Sakai, M., “An efficient multi-dimensional implementation of VSIAM3 and its applications to free surface flows,” *Phys. Fluids* **29**(12), 121611 (2017).
- <sup>43</sup>Yokoi, K., Onishi, R., Deng, X.-L., and Sussman, M., “Density-scaled balanced continuum surface force model with a level set based curvature interpolation technique,” *Int. J. Comput. Methods* **13**(4), 1641004 (2016).
- <sup>44</sup>Zalesak, S. T., “Fully multidimensional flux-corrected transport algorithms for fluids,” *J. Comput. Phys.* **31**(3), 335–362 (1979).